ACS APPLIED ENERGY MATERIALS

www.acsaem.org Article

# Bulky Cations Improve Band Alignment and Efficiency in Sn–Pb Halide Perovskite Solar Cells

Deepak Thrithamarassery Gangadharan, David Valverde-Chávez, Andrés-Felipe Castro-Méndez, Vivek Prakash, Ricardo Izquierdo, Carlos Silva, Dongling Ma,* and Juan-Pablo Correa-Baena*

Cite This: *ACS Appl. Energy Mater.* 2021, 4, 2616–2628 Read Online

ACCESS | Metrics & More | Article Recommendations | Supporting Information

**ABSTRACT:** The commercial feasibility of perovskite solar cells (PSCs) is not guaranteed as long as lead (Pb) is present in the active material, halide perovskites. Mixed halide tin (Sn)-based alloyed perovskites with optimal band gaps ranging from 1.15 to 3.55 eV are excellent alternatives to Pb-based perovskites. In this work, we find that the addition of a bulky phenylethyl ammonium (PEA) cation in the precursor solution leads to an improved solar cell performance and optoelectronic properties. A prolonged laser exposure is found to induce a redshift in the sample absorption for the control and no shift for the PEA-added sample, as shown by transient absorption spectroscopy. Further, we show that the addition of PEA improves band alignment of the perovskite with phenyl-$C_{61}$-butyric acid methyl ester, which aids in electron injection and therefore increases photocurrents in solar cells. Further, we show that PEA addition suppresses halide segregation improving material stability and recombination dynamics in the perovskite material. As a result, the PEA-containing Sn-rich PSCs exhibited a champion efficiency of 13% with an open-circuit voltage of 0.77 V and improved current–voltage hysteresis behavior. These results shed light on the importance of halide segregation and band alignment when designing lead-free PSCs.

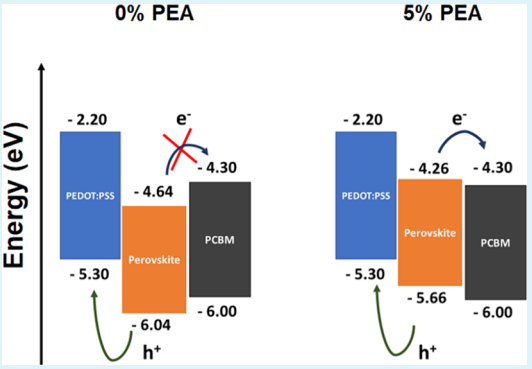


**KEYWORDS:** *perovskite solar cells, lead-free perovskites, compositional engineering, band alignment, Sn–Pb perovskites, transient absorption spectroscopy, photoinduced halide segregation*



## INTRODUCTION

With the recently certified power conversion efficiency (PCE) of 25.5%, halide perovskite solar cells (PSCs) are ready to match the performance of silicon (Si) and gallium arsenide (GaAs) thin-film photovoltaic technologies.[1] Nevertheless, the use of toxic lead (Pb) in state-of-the-art $ABX_3$ perovskites [where A = methylammonium (MA), formamidinium (FA), cesium (Cs) and/or rubidium (Rb); B = Pb and/or tin (Sn); X = chlorine (Cl), bromine (Br) and/or iodine (I)] is challenging in kickstarting large-scale production and commercialization of this new technology. Recent reports have shown the bioavailability of Pb from perovskites and their detrimental effects on plants.[2] On the other hand, Sn/germanium (Ge)-based perovskites, double perovskites such as $Cs_2AgBiBr_6$, $Cs_2AgBiCl_6$, $AgBi_2I_7$, and bismuth (Bi)/antimony (Sb)-based perovskite-like structures are some viable alternatives to the Pb-based perovskites.[3−8]

Among the Pb-free alternatives, Sn-based perovskites are the most attractive candidates because of their similar optoelectronic properties to those of the Pb-based counterparts.[9−12] With band gaps ranging from 1.15 to 3.55 eV, long-lived charge carriers, and high optical density, Sn-based perovskites should, in principle, be able to exhibit similar efficiencies to those of Pb-based perovskites. However, their performance is mainly limited by low open-circuit voltage ($V_{oc}$) because of high defect concentration in the material.[13,14] One of the main reasons for the poor $V_{oc}$ is unwanted oxidation of $Sn^{2+}$ to $Sn^{4+}$, which acts as a p-type dopant in the material.[15] To circumvent full oxidation of the perovskites, alloying of Sn with Pb has been used as a promising strategy toward achieving less toxic PSCs with device performances that approach those of the Pb-based counterparts. So far, halide Sn–Pb perovskites with ≤60% Sn of total B-site metal content deliver the highest efficiencies.[16,17] The performance of halide Sn–Pb perovskites with ≥60% Sn is partly limited by oxidization of $Sn^{2+}$ to $Sn^{4+}$, which generally reduces the $V_{oc}$ of PSCs.[18,19] In addition to being less toxic, the band gaps of Sn-based perovskites make them ideal for building perovskite–perovskite tandem solar cells.[20]

**Received:** December 23, 2020
**Accepted:** February 19, 2021
**Published:** March 3, 2021

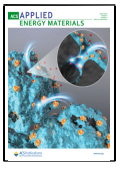





https://dx.doi.org/10.1021/acsaem.0c03191
*ACS Appl. Energy Mater.* 2021, 4, 2616–2628

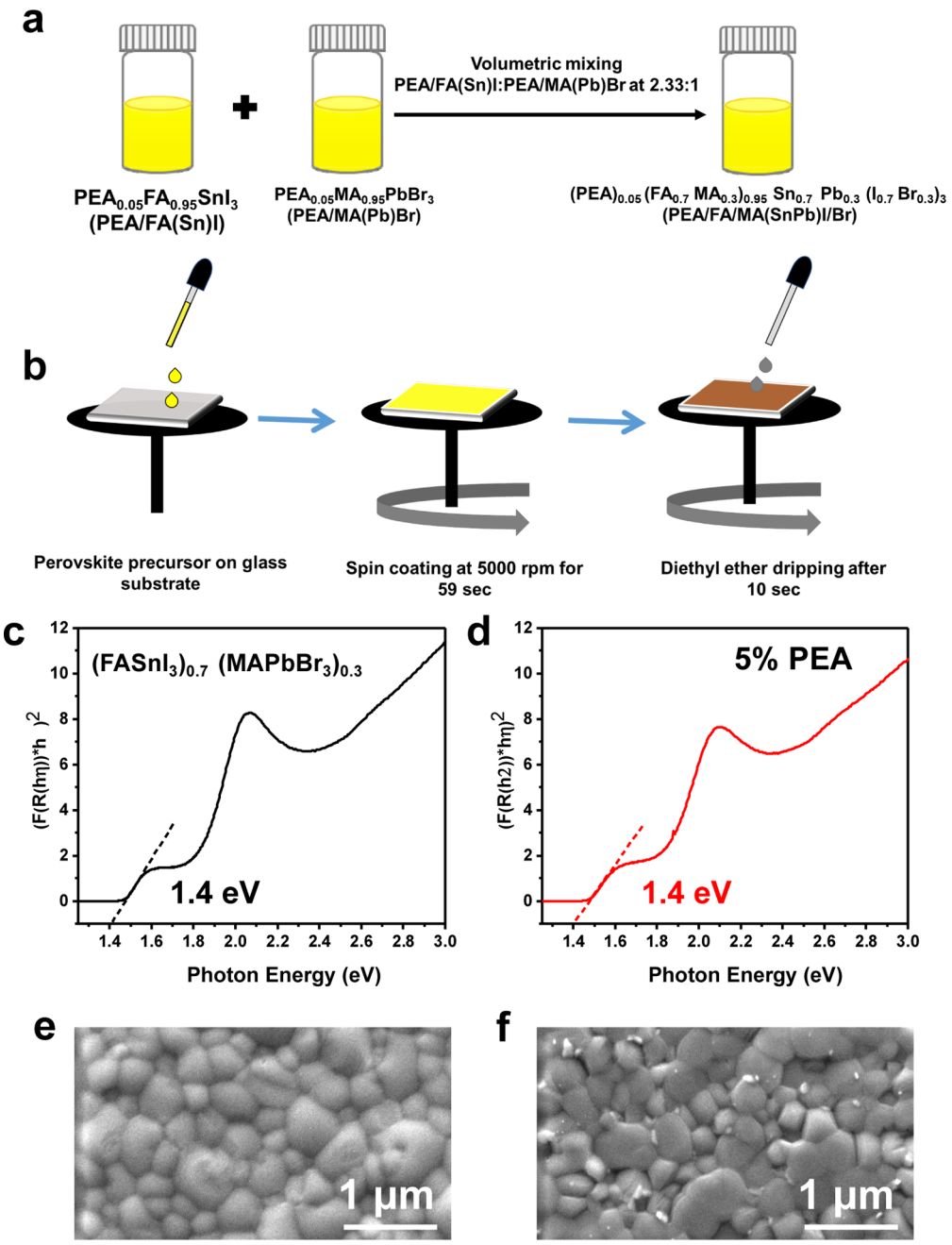


**Figure 1.** Perovskite thin-film deposition and its optical properties. (a) Schematic of preparation of the PEA/FA/MA(SnPb)I/Br perovskite precursor, (b) schematic of perovskite thin film fabrication, Tauc plots showing band gaps of (c) FA/MA(SnPb)I/Br and (d) PEA/FA/MA(SnPb)I/Br, and SEM images of (e) FA/MA(SnPb)I/Br and (f) PEA/FA/MA(SnPb)I/Br.

In this work, our primary objective was to design a less toxic perovskite material (by reducing the amount of Pb as low as possible) for a single-junction solar cell without much compromising photovoltaic performance. The Sn oxidation in narrow band gap Sn-rich perovskites reduces the $V_{oc}$ and photovoltaic performance of the devices. The band gap of the perovskite can be tuned by using fractional mixtures of I and Br in the composition, known as mixed halide perovskites.[21,22] The addition of Br to Sn−Pb perovskites is aimed at increasing the band gap of the material from 1.15 to 1.4 eV, as this yields a maximum in the theoretical efficiency calculated by Shockley−Queisser, while maintaining a relatively large $V_{oc}$. However, these mixtures are known to induce segregation of halides,[23−25] which is in turn responsible for low photovoltaic performance and stability of the devices.[26−28] The halide segregation involves many different processes, including light-induced halide ion migration, which leads to the formation of I-rich and Br-rich domains.[24] Recently, we have found that halide distribution becomes homogenized upon partial substitution of A-site cations with inorganic cations.[29] Recent record efficiency reports suggest that addition of bulky organic cations [such as phenylethyl ammonium (PEA), butylammonium, and guanidinium thiocyanate] in the perovskites leads to surface passivation, improved charge carrier lifetimes, and reduced ionic transport.[16,30−33]

In this work, we employ a mixed-halide Sn-rich alloyed perovskite (with 70% Sn and 30% Pb of total B-site metal content) with a band gap of 1.4 eV rather than the widely used


https://dx.doi.org/10.1021/acsaem.0c03191
ACS Appl. Energy Mater. 2021, 4, 2616−2628

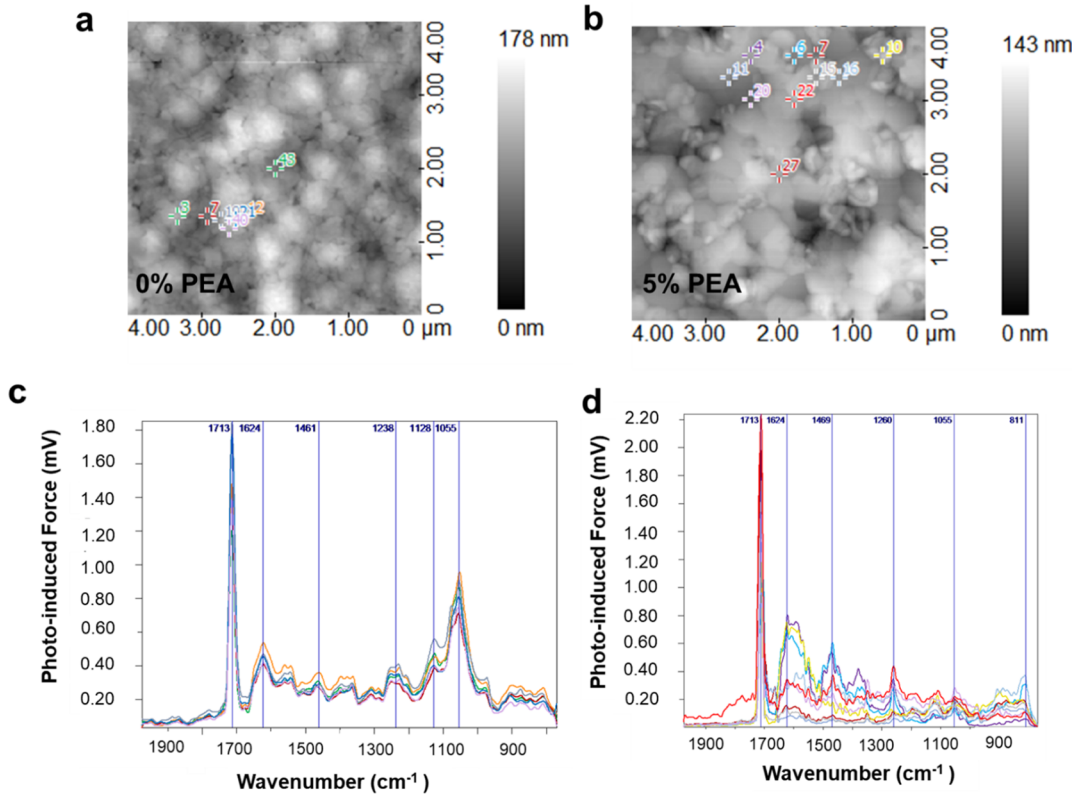


**Figure 2.** IR spectra of perovskite film surface topography of (a) FA/MA(SnPb)I/Br and (b) PEA/FA/MA(SnPb)I/Br perovskite films and their IR spectra in (c,d), respectively.

narrow band gap iodide-based alloyed perovskites. The mixed-halide Sn−Pb-alloyed perovskite thin films, $(FASnI_3)_{0.7}(MAPbBr_3)_{0.3}$ (FA/MA/SnPb/I/Br), are prepared from a mixture of $FASnI_3$ and $MAPbBr_3$ perovskite precursors. The 1.4 eV band gap of FA/MA/SnPb/I/Br is very close to the optimal band gap for achieving maximum theoretical efficiency in a single-junction solar cell.[20] However, this material showed poor solar cell performance, mainly because of inferior photocurrent, despite its impressive $V_{oc}$. The photoelectron spectroscopy revealed the metal halide inhomogeneity in FA/MA/SnPb/I/Br perovskite and their unfavorable band alignment with the electron selective layer, phenyl-$C_{61}$-butyric acid methyl ester (PCBM). The recombination dynamics in Sn-Pb alloyed perovskites were investigated through transient absorption (TA) measurements. A prolonged laser exposure on the FA/MA/SnPb/I/Br perovskite during the TA measurement led to a redshift of photobleach near the band gap, indicating occurance of photoinduced halide segregation in the samples. Here, we investigate the effects of adding bulky PEA cations in a perovskite composition on the distribution of metals and halides throughout the film, thereby achieving favorable band alignment with PCBM and reducing the photoinduced halide segregation in mixed halide Sn−Pb alloyed perovskites.

**Optical and Morphological Properties.** The FA/MA(SnPb)I/Br precursor solution is prepared by mixing $FASnI_3$ and $MAPbBr_3$ solutions (in dimethylformamide and dimethyl sulfoxide) at a 2.33:1 ratio. A 5% of PEA with respect to FA/MA was added to produce PEA/FA/MA(SnPb)I/Br precursor solution. A schematic of PEA/FA/MA(SnPb)I/Br precursor solution preparation is presented in Figure 1a. We prepared films of FA/MA(SnPb)I/Br and PEA/FA/MA(SnPb)I/Br using the commonly used antisolvent approach for Sn perovskites (Figure 1b).[34,35]

The thin films were prepared on a glass substrate for optical characterization. The absorption spectra of these films were measured, and the band gap was extracted for the FA/MA(SnPb)I/Br and PEA/FA/MA(SnPb)I/Br perovskites, as shown in Figure 1c,d. Generally, Sn−Pb-alloyed perovskites are narrow band gap semiconductors (~1.2 eV).[16,35,36] The presence of both Pb and Br in the mixed-halide Sn−Pb perovskites resulted in a wider band gap of 1.4 eV. Adding 5% of PEA to the FA/MA(SnPb)I/Br perovskite solution did not significantly change the band gap of the perovskite thin film (Figure 1d). We characterized the morphology by imaging the top view of the perovskite films prepared on a glass/poly(3,4-ethylene dioxythiophene)-poly (styrene sulfonate) (PEDOT:PSS) substrate by scanning electron microscopy (SEM; Figure 1e,f). The images show pinhole-free perovskite films with crystal grain sizes between 100 and 500 nm. Pinhole-free films with large grain sizes are highly desirable for efficient, hysteresis-free, and reproducible solar cells.[37,38] No significant changes in grain sizes were observed upon the addition of PEA. Both films showed a relatively broad distribution of grain sizes, which is not ideal for optoelectronic applications, and we anticipate that a further optimization of solvent and antisolvent engineering could result in larger grains with a more uniform distribution.[39] Besides, we observed small features on the perovskite film surface after the introduction of PEA. Following several literature reports, we initially anticipated that these small features could be 2D phases, formed as a consequence of the addition of PEA.[40,41] We tried to analyze small features on the perovskite film by performing atomic force microscopy integrated with infrared spectroscopy (AFM-IR or nano-IR)


https://dx.doi.org/10.1021/acsaem.0c03191
ACS Appl. Energy Mater. 2021, 4, 2616−2628

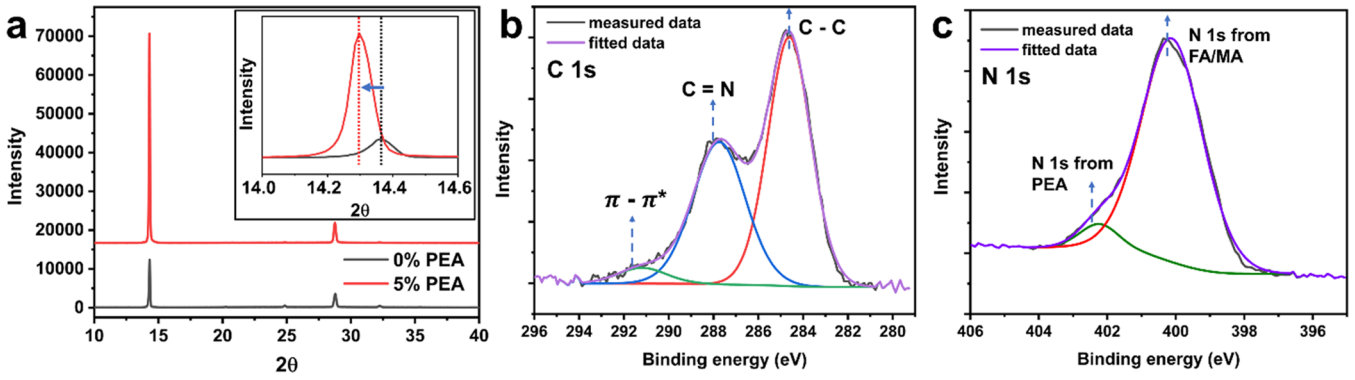


**Figure 3.** Structural properties and elemental composition of perovskite thin films. (a) Comparison of XRD spectra of FA/MA(SnPb)I/Br and PEA/FA/MA(SnPb)I/Br (inset: shift in major XRD peak) and high-resolution XPS spectra of (b) C 1s and (c) N 1s of PEA/FA/MA(SnPb)I/Br perovskites.

on perovskite film surfaces.[42] IR mapping allows us to analyze the chemical composition, specifically, organic components at a specific location of the perovskite film surface by investigating the IR signal from that site. Figure 2a,b shows the topography of perovskite films. IR spectra of marked spots on the perovskite film surface (see Figure 2a,b) are shown in Figure 2c,d. Both films showed a strong IR signal at 1713 $cm^{-1}$, which can be attributed to C═N symmetric stretching of the $FA^+$ cation.[43−45] The peak that appeared at 1461 $cm^{-1}$ is the characteristic $NH_3$ asymmetric bending mode, which suggests the presence of organic $MA^+$ cations in these samples. Additionally, the peaks observed in PEA/FA/MA(SnPb)I/Br samples around 1500 $cm^{-1}$ (at 1500 and 1469 $cm^{-1}$) are consistent with the presence of an aromatic compound.[46,47] Furthermore, the peak observed at 811 $cm^{-1}$ also corresponds to in-plane CH bending vibrations of aromatic compounds. These characteristic bands confirm the presence of PEA molecules on the perovskite surface. Here, we strategically chose locations [color-coded and cross-hair cursors (numbered) on AFM images specify the location where IR spectra were measured], such as grain boundaries, and observed small features on the surface to investigate the compositional/chemical nature of unique features.

The signals corresponding to PEA molecules are varied in intensity at different locations, but we observed no trend or pattern. For instance, location [10] positioned at a smaller feature does not show IR bands for PEA cations; conversely, the small feature observed at location [6] showed characteristic bands corresponding to PEA molecules. These results suggest that small features seen on PEA/FA/MA(SnPb)I/Br perovskite films are not exclusively 2D phases or PEA-containing perovskites. To sum up, a careful AFM-IR analysis revealed that these small features might be originating from a difference in crystallization induced by PEA, instead of a collection of 2D perovskite phase.

**Structural Properties.** To understand the structural changes to the perovskite films upon the addition of PEA, we performed X-ray diffraction (XRD) measurements. XRD results are presented in Figure 3a. A significant increase in the XRD peak intensity was observed for PEA/FA/MA(SnPb)I/Br samples compared to FA/MA(SnPb)I/Br, showing that PEA/FA/MA(SnPb)I/Br perovskites exhibit increased preferential orientation in the (110) plane than the counterparts without PEA. Adding PEA also led to formation of 2D perovskite phases, as evidenced by the emergence of a low angle peak around $2\theta$ = 3.5° (Figure S1).[48] Interestingly, we observed a shift in XRD peaks in these alloyed perovskites when we incorporated PEA, indicating an increase in lattice constants. The major peak located at 14.365° corresponding to the (110) crystal plane shifted to 14.297° when PEAI was added (see the inset of Figure 3a). Generally, incorporation of a cation with a large ionic radius into the structure increases the lattice constants. However, because of its larger size, we would not expect the PEA to be able to be integrated within the perovskite structure.[49] On the other hand, adding more iodine or homogenization of bromine with respect to iodine in mixed-halide perovskites, increases the lattice constant, as iodine expands the lattice. Peak profile analysis has shown that the addition of PEAI led to a slight decrease in the full width at half maximum (fwhm) (Figure S2).

The decrease in the fwhm implies a less strained lattice upon addition of 5% PEA. The reduction of fwhm of the (110), (200) peaks shows a lowering of the lattice strain along the inorganic bonding direction of I−Sn (and/or Pb)−I, Br−Pb (and/or Sn)−Br, or I−Pb (and/or Sn)−Br.[29]

**Chemical Compositional Analysis.** The elemental composition of perovskite films was probed by using XPS. The high-resolution spectra of various elements in perovskites are shown in Figures 3b,c, and S3−S5. The presence of PEA in PEA/FA/MA(SnPb)I/Br was confirmed by analyzing the C 1s and N 1s peaks (Figure 3b,c). The $\pi-\pi^*$ satellite peak observed at 291.2 eV around 6.4 eV from the main C 1s peak corresponds to the aromatic rings of the PEA molecule (Figure 3b). Furthermore, the MA, FA, and PEA can easily be distinguished from each other by the location of N 1s spectra (Figure S6). We have performed XPS and analyzed the N 1s peak of three different perovskite components [namely, $FASnI_3$, $MAPbBr_3$, and $(PEA)_2\ Sn_{0.7}\ Pb_{0.3}\ (I_{0.7}Br_{0.3})_4$ (pure 2D phase)] present in the PEA/FA/MA(SnPb)I/Br perovskite composition. $FASnI_3$, $MAPbBr_3$, and $(PEA)_2\ Sn_{0.7}\ Pb_{0.3}\ (I_{0.7}Br_{0.3})_4$ present a single N 1s peak located at ∼400.3, ∼400.5, and 401.7 eV, respectively. The peaks corresponding to MA and FA are close and not separable in FA/MA(SnPb)I/Br perovskite films (Figure S3b; located at 400.1 eV). On the other hand, the N 1s peak of the PEA/FA/MA(SnPb)I/Br perovskite (Figure 3c) can be deconvoluted into two peaks: (1) located at 402.2 eV corresponding to the N 1s peak from PEA and (2) located at 400.1 eV corresponding to the N 1s peak from FA/MA. To investigate the PEA distribution in the PEA/FA/MA/(SnPb)I/Br perovskite film, we analyzed C 1s and N 1s peaks after etching the film surface with 10 keV Ar 500 + ions (Figure 4). The $\pi-\pi^*$ satellite peak of C 1s observed at 291.2 eV and N 1s peak located at 402.2 eV from PEA were observed even after five etching cycles, suggesting that PEA molecules are distributed across the


https://dx.doi.org/10.1021/acsaem.0c03191
ACS Appl. Energy Mater. 2021, 4, 2616−2628

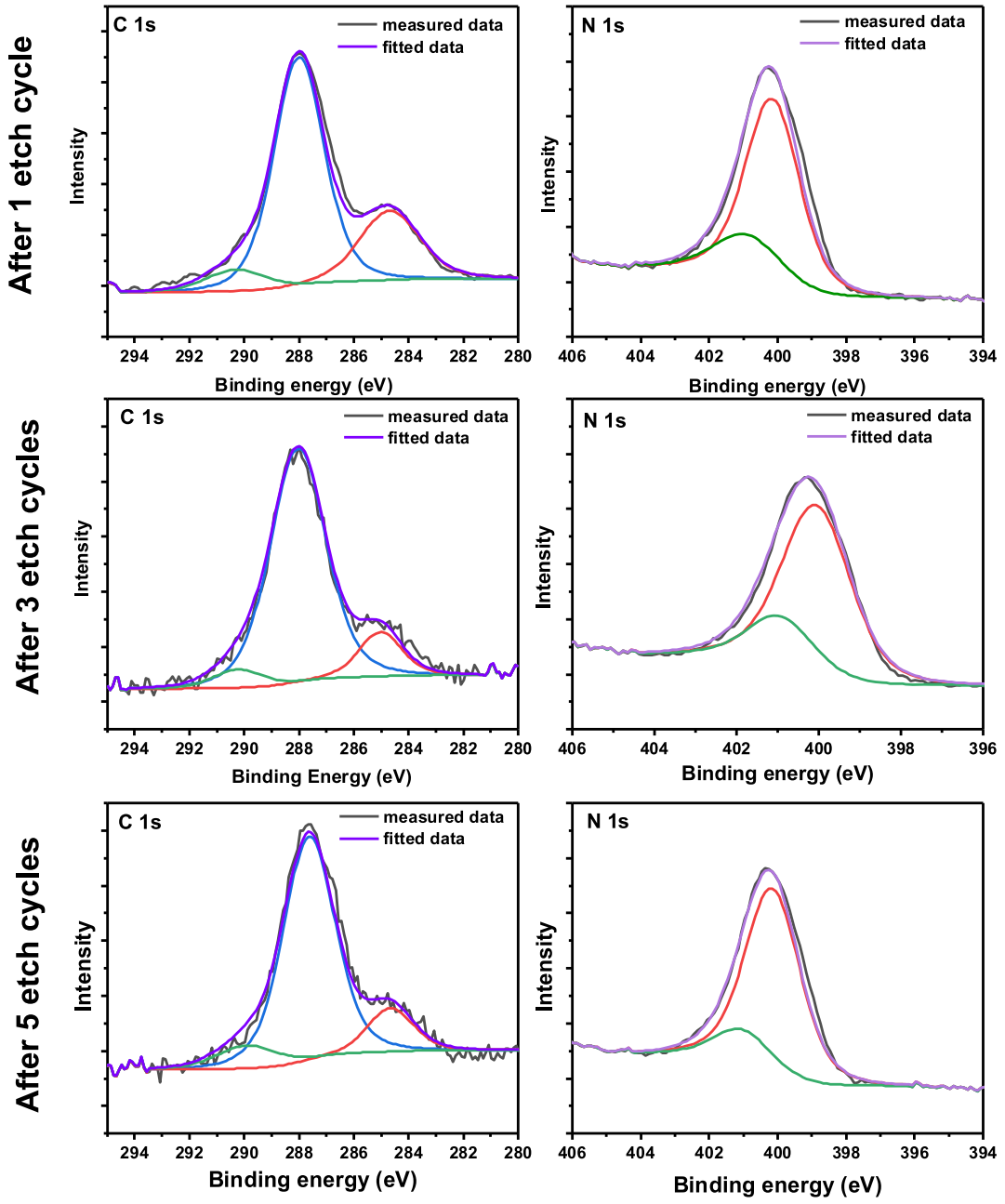


**Figure 4.** X-ray photoemission spectroscopy (XPS) depth profiling of perovskite films C 1s and N 1s XPS spectra of PEA/FA/MA(SnPb)I/Br perovskite films after etching the surface with 10 keV Ar ions.

film from the surface to bulk. However, the intensity of these peaks does not show any particular trend, which might be because the PEA molecules are randomly distributed across the film. As expected, FA/MA(SnPb)I/Br perovskite films did not show any of the peaks corresponding to PEA (Figure S3). Furthermore, we analyzed the chemical compositional differences between samples by quantifying XPS signal intensity ratios between different elements. The estimated intensity ratios from XPS compared to the ratios obtained from the chemical formula to investigate chemical compositions of thin films. Table 1 presents the Sn/Pb and I/Br ratios estimated from high-resolution XPS for the perovskites. The estimated Sn/Pb ratio from XPS for FA/MA(SnPb)I/Br perovskite is 3.90, which deviates from the theoretical value of 2.33. Because XPS is a surface-sensitive technique (less than 3 nm), a large deviation in

**Table 1. Intensity Ratios between Elements Calculated from XPS Spectra from Perovskites**

| composition | Sn/Pb (theoretical:2.33) | I/Br (theoretical:2.33) |
|---|---|---|
| FA/MA(SnPb)I/Br | 3.90 | 2.06 |
| PEA/FA/MA(SnPb)I/Br | 2.29 | 3.21 |

Sn/Pb ratio suggests a Sn-rich perovskite surface in FA/MA(SnPb)I/Br perovskite thin film. The estimated I/Br ratio, 2.06, for the FA/MA(SnPb)I/Br perovskite also differs from the theoretical value (2.33), obtained from a chemical formula suggesting an I-poor perovskite surface. In short, the FA/MA(SnPb)I/Br perovskite film has an Sn-rich and I-poor surface. This may be due to the inhomogeneous distribution of elements throughout the FA/MA(SnPb)I/Br perovskite thin



https://dx.doi.org/10.1021/acsaem.0c03191
ACS Appl. Energy Mater. 2021, 4, 2616−2628

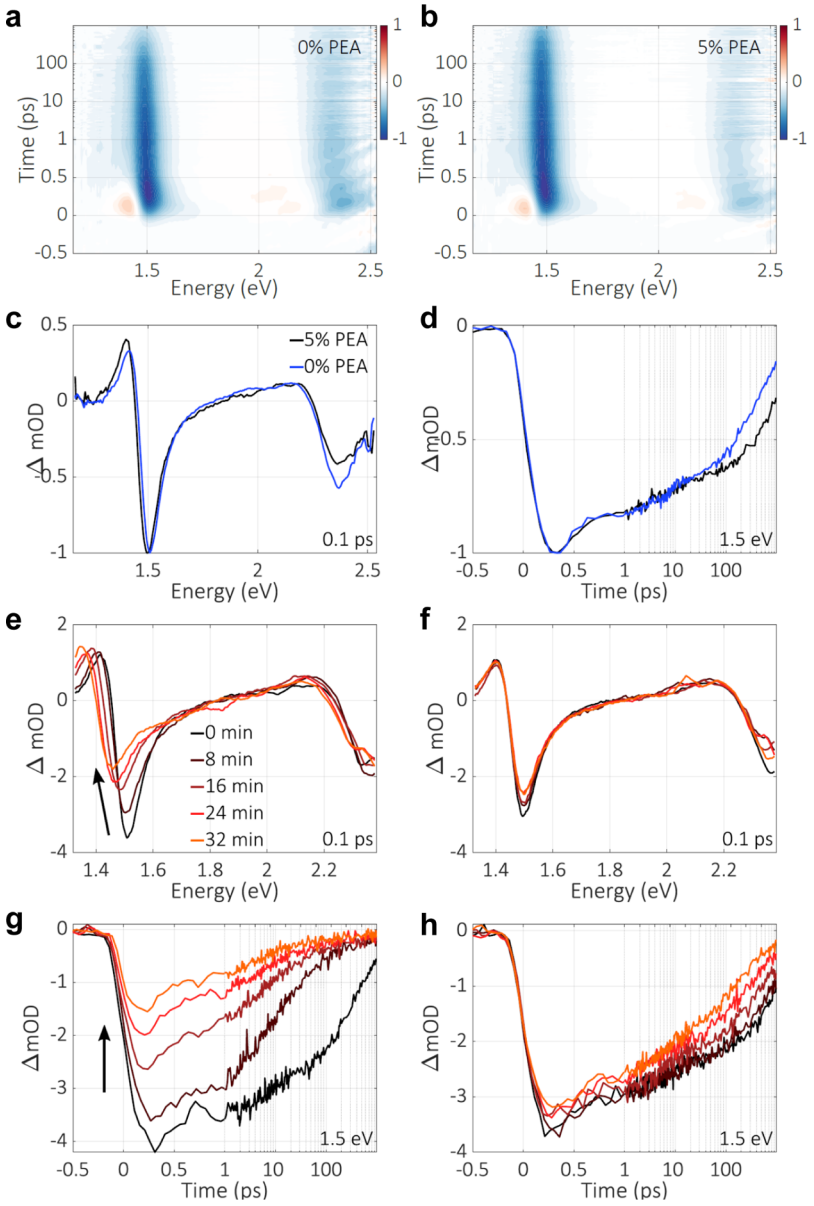


**Figure 5.** Charge carrier dynamics and optical properties of perovskite thin films (a) TA 2D maps of (a) FA/MA(SnPb)I/Br perovskite and (b) PEA/FA/MA(SnPb)I/Br perovskite on a glass substrate, (c) comparison of normalized TAS of FA/MA(SnPb)I/Br perovskite and PEA/FA/MA(SnPb)I/Br perovskite at 0.1 ps after excitation with a 2.7 eV laser pulse, and (d) comparison of time-dependent behavior of the normalized GSB + SE signals at 1.5 eV. (e) Evolution of TAS at 0.1 ps after pump excitation and white light (WL) probe exposure for FA/MA(SnPb)I/Br and (f) PEA/FA/MA(SnPb)I/Br perovskites. (g) Evolution of TAS dynamics at 1.5 eV after pump excitation and WL probe exposure for FA/MA(SnPb)I/Br and (h) PEA/FA/MA(SnPb)I/Br perovskites.

film. The addition of PEA changes the chemical composition of the perovskite film at the surface. The Sn/Pb ratio for PEA/FA/MA(SnPb)I/Br is close to the theoretical value, which is in agreement with the chemical formula (Table 1). However, the I/Br ratio for PEA/FA/MA(SnPb)I/Br varies from the theoretical value, making these films I-rich surfaces, which is consistent with the observed XRD peak shift. This suggests that a more homogenous metal distribution is present throughout the PEA/FA/MA(SnPb)I/Br perovskite film with I-rich surfaces. A simple explanation for the emergence of I-rich film surface can be derived from AFM-IR and XPS depth profiling, clearly showing a strong PEAI distribution on the film surface. We reason that the strong presence of PEAI salt on the film surfaces makes them I-rich surfaces. The change in I and Br distribution due to a less strained lattice in PEA-containing perovskites also cannot be discarded. Previously, we have shown that incorporating Rb and Cs cations lead to a less strained lattice and the modified distribution of I and Br.[29] The observed reduction in fwhm of the XRD peak in PEA-containing samples indicates a less strained lattice in the sample. We posit that PEA cations may have similar effects as Rb and Cs cations—a less strained lattice modifying the perovskite composition.

In our opinion, the two hypotheses mentioned above are not mutually exclusive, and instead, both less-strained lattice and PEAI salt distribution on the film surface can lead to the compositional changes in mixed-halide Sn−Pb perovskites. We also found a reduction of $Sn^{2+}$ oxidation to $Sn^{4+}$ after the addition of PEA in the perovskite composition (Figure S7). The $Sn^{2+}$ oxidation often leads to an increased nonradiative recombination in Sn-based perovskites, and partially hindering



https://dx.doi.org/10.1021/acsaem.0c03191
ACS Appl. Energy Mater. 2021, 4, 2616−2628

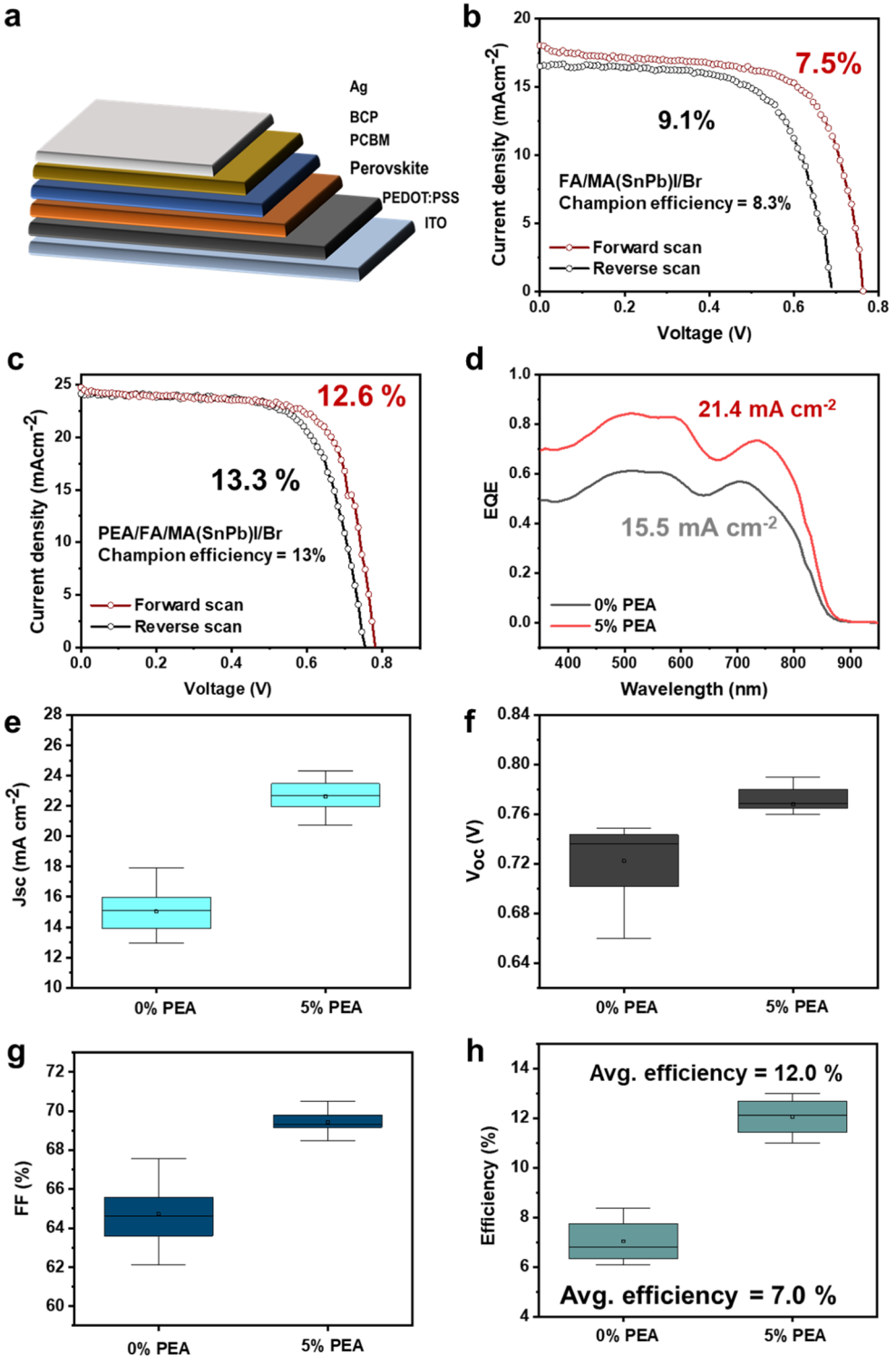


**Figure 6.** Solar cell configuration and characterization. (a) Schematic of the PSCs. (b) *J*–*V* curves of solar cells employing FA/MA(SnPb)I/Br and (c) PEA/FA/MA(SnPb)I/Br in PEDOT:PSS/perovskite/PCBM/BCP/Ag device configuration measured at a scan rate of 15 mV/s, (d) comparison of EQE spectra of FA/MA(SnPb)I/Br and PEA/FA/MA(SnPb)I/Br devices (calculated $J_{sc}$ from EQE presented in the graph), statistical values for (e) $V_{oc}$, (f) $J_{sc}$, (g) FF, and (h) efficiency from 21 devices per perovskite composition.

the $Sn^{2+}$ oxidation by adding PEA could improve the performance and stability of the material.

**Optoelectronic Properties.** To understand the recombination dynamics in mixed-halide alloyed perovskites, we studied the photophysical dynamics through TA spectroscopy (TAS), as shown in Figure 5. TAS measurements were performed on a perovskite/glass substrate to study carrier dynamics and the effects of prolonged photoirradiation in the neat mixed-halide alloyed perovskite films. In this scenario, we do not expect any quenching of the TA signal as the glass substrate does not act as a quencher. Pump pulses of 2.70 eV and ~220 fs with fluences of ~500 nJ/cm$^2$ were used to photoexcite into the conduction


https://dx.doi.org/10.1021/acsaem.0c03191
ACS Appl. Energy Mater. 2021, 4, 2616−2628

band (CB) of the perovskites. The two-dimensional TA maps for FA/MA(SnPb)I/Br and PEA/FA/MA(SnPb)I/Br (Figure 5a,b, respectively) present subtle differences. The dominant characteristic of the TAS spectra located around 1.5 eV can be assigned to a long-lived ground-state bleaching (GSB) and stimulated emission (SE).[50−52] Another weak GSB + SE region was observed above 2.2 eV. The presence of two distinct GSB + SE regions in halide perovskites has been attributed to electronic transition stemming from the perovskite's dual valence band composition. There is an ultrafast photoinduced absorption process that occurs at ∼1.4 eV, and this can be attributed to hot carrier cooling and band gap renormalization.[53] Finally, a short-lived (∼1 ps), weak photoinduced absorption spanning from ∼1.9 to 2.2 eV can be attributed to photoinduced refractive index changes and/or to transitions of free carriers from the CB edge to higher states within the CB and/or from lower valence bands (VBs) to the VB edge.[53,54] Figure 5c shows the TAS spectra at 0.1 ps normalized to the 1.5 eV peak for both perovskites. Although the spectral shape looks similar, the GSB + SE near the band gap is slightly red-shifted upon PEA addition, and it is in line with the study by Shao et al.[55] The observed redshift could be a result of compositional changes such as I-rich surfaces in PEA/FA/MA(SnPb)I/Br perovskite films, as we noted in XPS analysis.

The time-dependent behavior of the normalized GSB + SE signal at 1.5 eV is shown in Figure 5d. The GSB + SE recovery of the PEA/FA/MA(SnPb)I/Br sample is slightly slower compared to FA/MA(SnPb)I/Br sample, suggesting a slower charge carrier depopulation in PEA-containing samples. Slow GSB + SE signal recovery in TAS implies a long-lived charge carrier population and longer diffusion length in the perovskite semiconductor. Compositional inhomogeneity and lattice strain can instigate nonradiative losses in these mixed halide perovskite films.[56]

Further measurements were performed to study the evolution under light exposure, where both pump light and probe light were continuously impinging the sample for over 30 min in a new spot. The FA/MA(SnPb)I/Br sample presents both a decrease and a redshift of the bleach near the band gap (Figure 5e). The light-induced redshift is often attributed to phase segregation in the mixed-halide perovskite.[28,57] The dynamics (Figure 5g) show a decrease in the GSB + SE intensity, mainly because of the phase segregation as well as degradation of the material, and the dynamics are reduced from hundreds of ps at the beginning of the measurement to only tens of ps after 30 min exposure to light. Although the photoinduced halide segregation is quite common in mixed-halide perovskites, the exact mechanism behind this phenomenon remains unknown.[58] Strain- or carrier-induced lattice distortion, compositional inhomogeneity, and defect-mediated halide migration are actively considered as contributing factors to cause photo-induced halide segregation.[23,28]

The incorporation of PEA into the perovskite presents a different scenario after 30 min of light exposure (Figure 5f). There is no evident peak shift of the 1.5 eV feature, and there is only a slight degradation of the GSB + SE peaks. Furthermore, the dynamics become slower but still in the hundreds of ps range (Figure 5h). This is a piece of clear evidence that the addition of PEA makes the perovskite structure more robust and less prone to photoinduced degradation. We hypothesize that better compositional homogeneity and reduced lattice strain induced by PEA led to less halide segregation in PEA/FA/MA(SnPb)I/Br perovskite materials.

**Solar Cell Performance.** The photovoltaic properties of FA/MA(SnPb)I/Br and PEA/FA/MA(SnPb)I/Br perovskites were evaluated in a planar solar cell architecture consisting of indium-doped tin oxide/PEDOT:PSS/perovskite/PCBM/bathocuproine (BCP)/silver (Ag) (Figure 6a). The current density−voltage ($J$−$V$) curves and external quantum efficiencies (EQEs) of champion devices are shown in Figure 6b−d, respectively. FA/MA(SnPb)I/Br devices exhibited an average PCE of 7.03 ± 0.70% with an open-circuit voltage ($V_{oc}$) of 0.72 ± 0.03 V, a short-circuit current density ($J_{sc}$) of 15.03 ± 1.35 mA cm$^{-2}$, and a fill factor (FF) of 64.73 ± 1.36%. It should be mentioned that the $V_{oc}$ reported here for FA/MA(SnPb)I/Br devices is among the highest for a Sn-rich alloyed PSC. Table S1 lists the highest $V_{oc}$ reported in the literature for Sn-containing (with a focus on Sn-rich compositions) devices. The high $V_{oc}$ in mixed-halide-based alloyed perovskite system (FA/MA(SnPb)-I/Br) is a result of a wider band gap (1.4 eV) and reduced recombination dynamics of this material. We are aware of only one report with similar $V_{oc}$ (0.76 V) for a Sn-rich perovskite composition ($FA_{0.8}Cs_{0.2}Sn_{0.7}Pb_{0.3}I_3$), where the authors used Cs to tune the band gap of the material *via* octahedral tilting.[59]

The addition of 5% PEA yields a significant enhancement in the overall device performance. PEA/FA/MA(SnPb)I/Br devices exhibited an average PCE of 12.06 ± 0.62% with $V_{oc}$ of 0.76 ± 0.01 V, $J_{sc}$ of 22.61 ± 1.06 mA cm$^{-2}$, and FF of 69.42 ± 0.78%. Figure 6e−g shows a box plot of summarizing the photovoltaic parameters obtained for FA/MA(SnPb)I/Br and PEA/FA/MA(SnPb)I/Br devices from 21 devices per perovskite compound. We noticed a slight current mismatch between $J$−$V$ and EQE measurements. The current mismatch is quite a common issue in PSCs. A broad range of reasons that are peculiar to perovskite materials ranging from ion migration to strong frequency dependence of the EQE for PSCs are posited as reasons for the mismatch.[60,61] Therefore, a current mismatch of 10−20% is typically observed for PSCs. In this report, the current density mismatch is around 12%, which is within the allowed range. We have also tried a higher amount of PEA (*i.e.,* 10%) in the composition and found an inferior PV performance compared to 5% of PEA (Table S2). All the photovoltaic parameters were improved in PEA/FA/MA(SnPb)I/Br devices compared to FA/MA(SnPb)I/Br devices, with the $J_{sc}$ showing the most substantial enhancement. The enhancement in $J_{sc}$ was also reflected in the EQE, which is the ratio of the number of photons to the number of generated charge carriers in a solar cell. The FF depends in part on the band alignment at perovskite/PEDOT:PSS and perovskite/PCBM interfaces. The origin of voltage loss in mixed-halide perovskites often attributed to a photoinduced halide segregation.[23,58,62] In that scenario, halide segregation under illumination causes the formation of Br-rich (I-poor) or I-rich (Br-poor) domains in mixed-halide perovskites, which facilitates recombination and limits the $V_{oc}$ of the solar cells.[63] We also see an increase in the $V_{oc}$ in PEA/FA/MA(SnPb)I/Br devices in conjunction with reduced halide segregation (TAS results) in perovskite films.

Contrary to popular belief, a recent study by Snaith et al. has shown that the $V_{oc}$ loss is due to the relatively low radiative efficiency of the solar cells (resulting from recombination originating both at the absorber layer and at the perovskite/charge selective layer) rather than from photo-induced halide segregation.[64] These contradicting reports indicate that voltage loss in mixed-halide perovskites is more complicated than what was previously thought, which suggests that more careful studies are needed to uncover the exact mechanism behind $V_{oc}$ loss in


https://dx.doi.org/10.1021/acsaem.0c03191
ACS Appl. Energy Mater. 2021, 4, 2616−2628

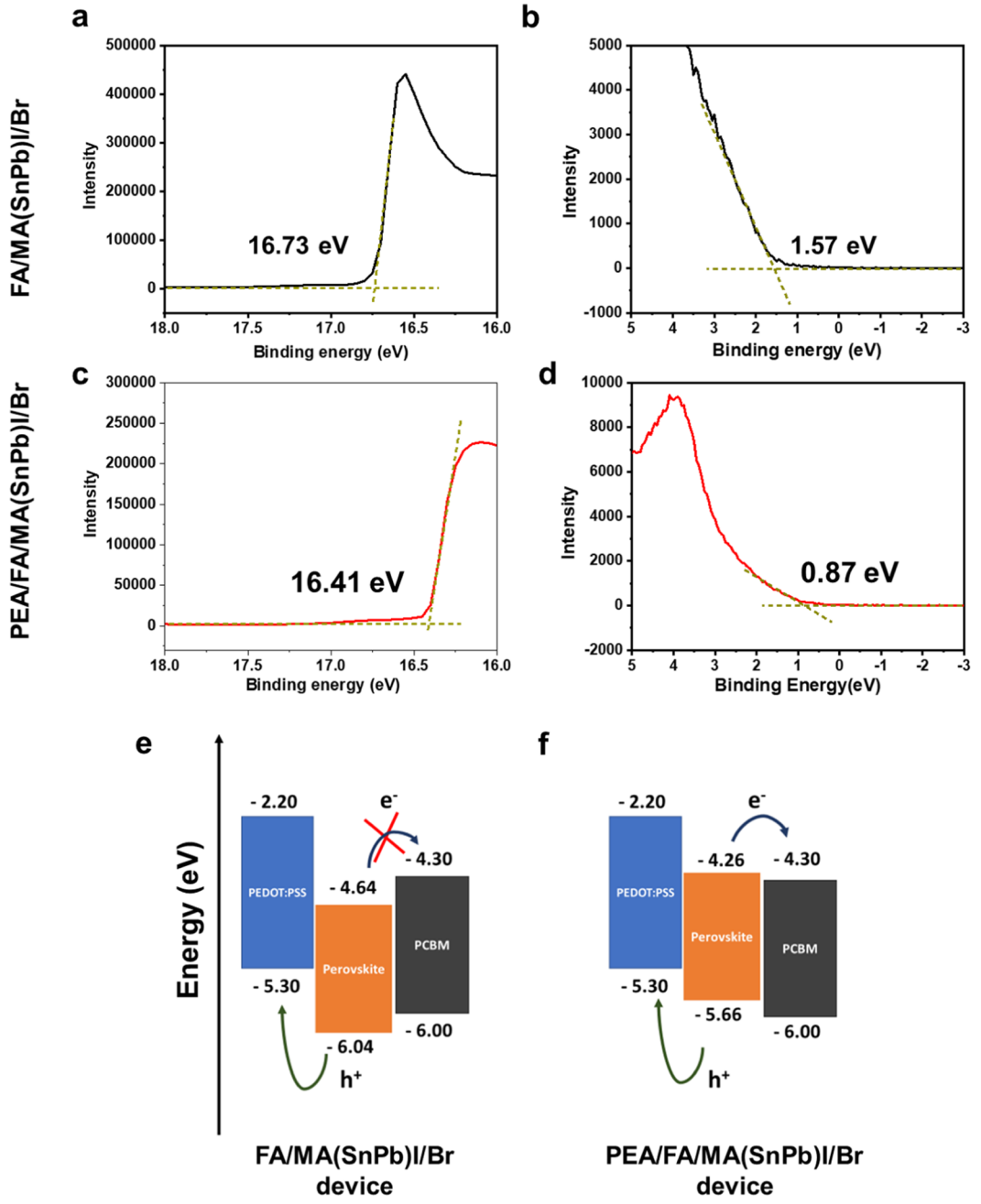


**Figure 7.** Ionization energies and band alignment of perovskites. (a) High energy cutoff and (b) low energy cut-off of UPS spectra for the FA/MA(SnPb)I/Br perovskite, (c) high energy cut-off and (d) low energy cutoff of UPS spectra for the PEA/FA/MA(SnPb)I/Br perovskite, and band alignment diagrams of (e) FA/MA(SnPb)I/Br device and (f) PEA/FA/MA(SnPb)I/Br device.

mixed-halide perovskite devices. Therefore, the $V_{oc}$ improvement in PEA/FA/MA(SnPb)I/Br devices could have multiple origins, such as reduced photoinduced halide segregation and/or reduced recombination in perovskite materials and at the perovskite/charge selective layer interfaces.

The devices exhibited improved $J-V$ hysteresis for the PEA/FA/MA(SnPb)I/Br materials. For instance, the PEA/FA/MA(SnPb)I/Br champion device demonstrated a PCE of 13.3% in the reverse scan and 12.6% in the forward scan, while the FA/MA(SnPb)I/Br champion device exhibited a more considerable hysteresis with a PCE of 9.1% in the reverse scan and 7.5% in the forward scan (Figure 6b,c). The hysteresis index (H-index) = $(PCE_{forward} - PCE_{reverse}/PCE_{reverse}) \times 100$, a metric to measure the severity of $J-V$ hysteresis, is used to compare both systems. The FA/MA(SnPb)I/Br device shows a high H-index of 21%, while the PEA/FA/MA(SnPb)I/Br device shows an H-index of 8%.

We also found slightly better shelf stability for PEA/FA/MA(SnPb)I/Br perovskite devices compared to FA/MA-(SnPb)I/Br perovskite devices (Figure S8). FA/MA(SnPb)I/Br perovskite devices completely degraded after 170 h, whereas the PEA-containing perovskite devices were operational after more than 200 h. This is indicative of Sn-rich perovskites being very prone to degradation against moisture. XPS has shown lower $Sn^{2+}$ oxidation in freshly prepared PEA-containing samples than the control sample (Figure S7), which could be one reason for the better stability of PEA-containing perovskite devices. In addition to $Sn^{2+}$ oxidation, the perovskite/charge-



https://dx.doi.org/10.1021/acsaem.0c03191
ACS Appl. Energy Mater. 2021, 4, 2616−2628

selective layer interfaces also contribute to the Sn−Pb perovskite device's degradation.

**Interfacial Energetics.** The substantial increase in $J_{sc}$ in PEA/FA/MA(SnPb)I/Br devices motivated us to investigate band alignment of perovskites with charge selective layers, as this has been observed to influence the photocurrent of devices heavily.[65] Ultraviolet photoemission spectroscopy (UPS) was performed on FA/MA(SnPb)I/Br and PEA/FA/MA(SnPb)I/Br perovskites to understand the ionization energy (with respect to vacuum) and therefore the VBM of these compounds (Figure 7a−d). The PEA/FA/MA(SnPb)I/Br showed lower ionization energy compared to that of FA/MA(SnPb)I/Br (−5.66 vs −6.04 eV, respectively). As we have noted in the XPS and XRD discussion, the precise chemical composition may be different in PEA/FA/MA(SnPb)I/Br compared to FA/MA(SnPb)I/Br, which may result in changes in the VBM position of the material. We reason that I-poor (and potentially Br-rich) perovskite surfaces of FA/MA(SnPb)I/Br, as seen in the XPS analysis, influence the energetic position of the VBM, as Br perovskites exhibit significantly higher ionization energy (and therefore deeper VBMs).[66] Our observation is in line with the DFT calculations performed by Beljonne et al., where authors have shown that perovskite film surface termination plays a critical role in determining the VBM and conduction band minima (CBM) energy levels.[67] Besides, Wang et al. recently reported a similar effect on mixed-halide Pb perovskites upon addition of *n*-propylammonium spacer cations, showing a CBM upshift of 0.16 eV.[68] To construct a CB alignment with the electron selective contact, we added the optical band gap to the ionization energy of the compounds and the known energy levels of PCBM[69] and PEDOT:PSS[70] and sketched it in Figure 7e,f. Because of a deeper VBM, the CBM of FA/MA(SnPb)I/Br has an unfavorable band alignment with PCBM creating an energy barrier of approximately 0.3 eV for the electron transport across the perovskite/PCBM interface. In contrast, the CBM of PEA/FA/MA(SnPb)I/Br aligns well with that of PCBM, with no apparent barrier across the perovskite/PCBM interface. Table 1 presents that the PEA/FA/MA(SnPb)I/Br perovskite has an I-rich surface, which pushes the CBM of the perovskite higher, reducing the energetic barrier at the interface. Energetic barriers at the electron-selective contact/perovskite interface have been shown to cause low $J_{sc}$ and increased the H-index in PSCs.[65] While the favorable band alignment across perovskite/PCBM boosts the $J_{sc}$ in PEA/FA/MA(SnPb)I/Br solar cells, the CBM misalignment with PCBM inhibits interfacial charge transfer in FA/MA(SnPb)I/Br solar cells, which in turn reduces the $J_{sc}$ in the devices.

The efficiency of interfacial charge transfer also affects the *J*−*V* hysteretic behavior in the device. The energy barrier at the perovskite/PCBM interface leads to the accumulation of charges at the interface, inducing a high electric field and/or dipole formation, causing a large *J*−*V* hysteresis in the device.[65] Improved *J*−*V* hysteretic behavior in PEA/FA/MA(SnPb)I/Br solar cells can be linked to an efficient charge collection at the perovskite/PCBM interface.

## CONCLUSIONS

In this work, we found that unfavorable band alignment at the mixed-halide Sn−Pb perovskite/PCBM interface resulting from compositional inhomogeneity is mainly responsible for its lower solar cell performance. Photoelectron spectroscopy and TA results reveal that the addition of bulky PEA cations in mixed-halide Sn−Pb perovskites invokes compositional changes and reduces the $Sn^{2+}$ oxidation in the material. The compositional changes in PEA-containing mixed-halide Sn−Pb perovskites present a favorable band alignment across the perovskite/PCBM, improving the photocurrent, FF, and *J*−*V* hysteretic behavior in the solar cells. The TAS measurements showed the suppression of light-induced halide segregation upon the addition of PEA in mixed-halide Sn−Pb perovskites, which indicate improved stability of the material. In summary, we investigated the beneficial effects of incorporating bulky organic cations into mixed-halide Sn−Pb perovskites and their impact on the performance of Sn-based mixed halide PSCs.

## ASSOCIATED CONTENT

### Supporting Information

The Supporting Information is available free of charge at https://pubs.acs.org/doi/10.1021/acsaem.0c03191.

Experimental methods and various characterization results, including XRD, X-ray photoelectron spectroscopy, and TA (PDF)

## AUTHOR INFORMATION


### Corresponding Authors

**Dongling Ma** − *Institut National de la Recherche Scientifique, Centre-Énergie Matériaux et Télécommunications, Université du Québec, Varennes, Québec J3X 1S2, Canada;* orcid.org/0000-0001-8558-3150; Email: ma@emt.inrs.ca

**Juan-Pablo Correa-Baena** − *School of Materials Science and Engineering, Georgia Institute of Technology, Atlanta, Georgia 30332, United States;* orcid.org/0000-0002-3860-1149; Email: jpcorrea@gatech.edu; @jpcorreabaena

### Authors

**Deepak Thrithamarassery Gangadharan** − *Institut National de la Recherche Scientifique, Centre-Énergie Matériaux et Télécommunications and Department of Electrical Engineering, École de technologie supérieure, Université du Québec, Varennes, Québec J3X 1S2, Canada; School of Materials Science and Engineering, Georgia Institute of Technology, Atlanta, Georgia 30332, United States;* orcid.org/0000-0002-7408-2278

**David Valverde-Chávez** − *School of Chemistry and Biochemistry, Georgia Institute of Technology, Atlanta, Georgia 30332, United States*

**Andrés-Felipe Castro-Méndez** − *School of Materials Science and Engineering, Georgia Institute of Technology, Atlanta, Georgia 30332, United States*

**Vivek Prakash** − *School of Materials Science and Engineering and School of Chemical and Biomolecular Engineering, Georgia Institute of Technology, Atlanta, Georgia 30332, United States*

**Ricardo Izquierdo** − *Department of Electrical Engineering, École de technologie supérieure, Université du Québec, Montréal, Québec H3C 1K3, Canada*

**Carlos Silva** − *School of Chemistry and Biochemistry and School of Physics, Georgia Institute of Technology, Atlanta, Georgia 30332, United States;* orcid.org/0000-0002-3969-5271

Complete contact information is available at: https://pubs.acs.org/10.1021/acsaem.0c03191


### Notes

The authors declare no competing financial interest.



https://dx.doi.org/10.1021/acsaem.0c03191
ACS Appl. Energy Mater. 2021, 4, 2616−2628

## ■ ACKNOWLEDGMENTS

J.-P.C.-B. acknowledges funding support from the School of Materials Science and Engineering and the College of Engineering at Georgia Tech. Financial support from the Natural Sciences and Engineering Research Council (NSERC) of Canada in the context of a NSREC Discovery Grant and a NSERC Strategic Grant (Industry partner: Canadian Solar Inc.) is greatly appreciated. D.M. is also grateful for the financial support from Quebec Center for Functional Materials (CQMF), Canada and from Canada Research Chair program. D.T.G. acknowledges scholarship support from the Fonds de recherche du Québec-Nature et technologies (FRQNT) for the Bourses de recherche en énergie/Doctorat (PhD Energy Research Scholarship) and Stages internationaux-Énergie-Numérique-Aérospatiale (International internship Scholarship-Energy-Digital-Aerospace). A.-F.C.-M. acknowledges the funding from Fulbright and Colciencias. C.S. acknowledges funding by the National Science Foundation (DMR-1904293) and support from the School of Chemistry and Biochemistry and the College of Science at Georgia Tech.

## ■ REFERENCES

(1) Best Research-Cell Efficiency Chart, https://www.nrel.gov/pv/cell-efficiency.html (accessed on February, 2021).
(2) Li, J.; Cao, H.-L.; Jiao, W.-B.; Wang, Q.; Wei, M.; Cantone, I.; Lü, J.; Abate, A. Biological Impact of Lead from Halide Perovskites Reveals the Risk of Introducing a Safe Threshold. *Nat. Commun.* **2020**, *11*, 310.
(3) Liang, L.; Gao, P. Lead-Free Hybrid Perovskite Absorbers for Viable Application: Can We Eat the Cake and Have It Too? *Adv. Sci.* **2018**, *5*, 1700331.
(4) Ke, W.; Stoumpos, C. C.; Kanatzidis, M. G. "Unleaded" Perovskites: Status Quo and Future Prospects of Tin-Based Perovskite Solar Cells. *Adv. Mater.* **2019**, *31*, 1803230.
(5) Igbari, F.; Wang, R.; Wang, Z.-K.; Ma, X.-J.; Wang, Q.; Wang, K.-L.; Zhang, Y.; Liao, L.-S.; Yang, Y. Composition Stoichiometry of $Cs_2AgBiBr_6$ Films for Highly Efficient Lead-Free Perovskite Solar Cells. *Nano Lett.* **2019**, *19*, 2066−2073.
(6) McClure, E. T.; Ball, M. R.; Windl, W.; Woodward, P. M. $Cs_2AgBiX_6$ (X = Br, Cl): New Visible Light Absorbing, Lead-Free Halide Perovskite Semiconductors. *Chem. Mater.* **2016**, *28*, 1348−1354.
(7) Sun, S.; Hartono, N. T. P.; Ren, Z. D.; Oviedo, F.; Buscemi, A. M.; Layurova, M.; Chen, D. X.; Ogunfunmi, T.; Thapa, J.; Ramasamy, S.; Settens, C.; DeCost, B. L.; Kusne, A. G.; Liu, Z.; Tian, S. I. P.; Peters, I. M.; Correa-Baena, J.-P.; Buonassisi, T. Accelerated Development of Perovskite-Inspired Materials via High-Throughput Synthesis and Machine-Learning Diagnosis. *Joule* **2019**, *3*, 1437−1451.
(8) Hu, Y.; Bai, F.; Liu, X.; Ji, Q.; Miao, X.; Qiu, T.; Zhang, S. Bismuth Incorporation Stabilized $\alpha$-$CsPbI_3$ for Fully Inorganic Perovskite Solar Cells. *ACS Energy Lett.* **2017**, *2*, 2219−2227.
(9) Noel, N. K.; Stranks, S. D.; Abate, A.; Wehrenfennig, C.; Guarnera, S.; Haghighirad, A.-A.; Sadhanala, A.; Eperon, G. E.; Pathak, S. K.; Johnston, M. B.; Petrozza, A.; Herz, L. M.; Snaith, H. J. Lead-Free Organic-Inorganic Tin Halide Perovskites for Photovoltaic Applications. *Energy Environ. Sci.* **2014**, *7*, 3061−3068.
(10) Ke, W.; Kanatzidis, M. G. Prospects for Low-Toxicity Lead-Free Perovskite Solar Cells. *Nat. Commun.* **2019**, *10*, 965.
(11) Abate, A. Perovskite Solar Cells Go Lead Free. *Joule* **2017**, *1*, 659−664.
(12) Anaya, M.; Correa-Baena, J. P.; Lozano, G.; Saliba, M.; Anguita, P.; Roose, B.; Abate, A.; Steiner, U.; Grätzel, M.; Calvo, M. E.; Hagfeldt, A.; Míguez, H. Optical Analysis of $CH_3NH_3Sn_xPb_{1-x}I_3$ Absorbers: A Roadmap for Perovskite-on-Perovskite Tandem Solar Cells. *J. Mater. Chem. A* **2016**, *4*, 11214−11221.
(13) Yokoyama, T.; Song, T.-B.; Cao, D. H.; Stoumpos, C. C.; Aramaki, S.; Kanatzidis, M. G. The Origin of Lower Hole Carrier Concentration in Methylammonium Tin Halide Films Grown by a Vapor-Assisted Solution Process. *ACS Energy Lett.* **2017**, *2*, 22−28.
(14) Song, T.-B.; Yokoyama, T.; Logsdon, J.; Wasielewski, M. R.; Aramaki, S.; Kanatzidis, M. G. Piperazine Suppresses Self-Doping in CsSnI 3 Perovskite Solar Cells. *ACS Appl. Energy Mater.* **2018**, *1*, 4221−4226.
(15) Takahashi, Y.; Obara, R.; Lin, Z.-Z.; Takahashi, Y.; Naito, T.; Inabe, T.; Ishibashi, S.; Terakura, K. Charge-Transport in Tin-Iodide Perovskite $CH_3NH_3SnI_3$: Origin of High Conductivity. *Dalton Trans.* **2011**, *40*, 5563−5568.
(16) Tong, J.; Song, Z.; Kim, D. H.; Chen, X.; Chen, C.; Palmstrom, A. F.; Ndione, P. F.; Reese, M. O.; Dunfield, S. P.; Reid, O. G.; Liu, J.; Zhang, F.; Harvey, S. P.; Li, Z.; Christensen, S. T.; Teeter, G.; Zhao, D.; Al-Jassim, M. M.; van Hest, M. F. A. M.; Beard, M. C.; Shaheen, S. E.; Berry, J. J.; Yan, Y.; Zhu, K. Carrier Lifetimes of >1 $\mu$s in Sn-Pb Perovskites Enable Efficient All-Perovskite Tandem Solar Cells. *Science* **2019**, *364*, 475−479.
(17) Prasanna, R.; Leijtens, T.; Dunfield, S. P.; Raiford, J. A.; Wolf, E. J.; Swifter, S. A.; Werner, J.; Eperon, G. E.; de Paula, C.; Palmstrom, A. F.; Boyd, C. C.; van Hest, M. F. A. M.; Bent, S. F.; Teeter, G.; Berry, J. J.; McGehee, M. D. Design of Low Bandgap Tin−Lead Halide Perovskite Solar Cells to Achieve Thermal, Atmospheric and Operational Stability. *Nat. Energy* **2019**, *4*, 939−947.
(18) Zhao, B.; Abdi-Jalebi, M.; Tabachnyk, M.; Glass, H.; Kamboj, V. S.; Nie, W.; Pearson, A. J.; Puttisong, Y.; Gödel, K. C.; Beere, H. E.; Ritchie, D. A.; Mohite, A. D.; Dutton, S. E.; Friend, R. H.; Sadhanala, A. High Open-Circuit Voltages in Tin-Rich Low-Bandgap Perovskite-Based Planar Heterojunction Photovoltaics. *Adv. Mater.* **2017**, *29*, 1604744.
(19) Tavakoli, M. M.; Zakeeruddin, S. M.; Grätzel, M.; Fan, Z. Large-Grain Tin-Rich Perovskite Films for Efficient Solar Cells via Metal Alloying Technique. *Adv. Mater.* **2018**, *30*, 1705998.
(20) Shockley, W.; Queisser, H. J. Detailed Balance Limit of Efficiency of P-n Junction Solar Cells. *J. Appl. Phys.* **1961**, *32*, 510−519.
(21) Eperon, G. E.; Stranks, S. D.; Menelaou, C.; Johnston, M. B.; Herz, L. M.; Snaith, H. J. Formamidinium Lead Trihalide: A Broadly Tunable Perovskite for Efficient Planar Heterojunction Solar Cells. *Energy Environ. Sci.* **2014**, *7*, 982−988.
(22) Jeon, N. J.; Noh, J. H.; Yang, W. S.; Kim, Y. C.; Ryu, S.; Seo, J.; Seok, S. I. Il. Compositional Engineering of Perovskite Materials for High-Performance Solar Cells. *Nature* **2015**, *517*, 476−480.
(23) Barker, A. J.; Sadhanala, A.; Deschler, F.; Gandini, M.; Senanayak, S. P.; Pearce, P. M.; Mosconi, E.; Pearson, A. J.; Wu, Y.; Srimath Kandada, A. R.; Leijtens, T.; De Angelis, F.; Dutton, S. E.; Petrozza, A.; Friend, R. H. Defect-Assisted Photoinduced Halide Segregation in Mixed-Halide Perovskite Thin Films. *ACS Energy Lett.* **2017**, *2*, 1416−1424.
(24) Yoon, S. J.; Kuno, M.; Kamat, P. V. Shift Happens. How Halide Ion Defects Influence Photoinduced Segregation in Mixed Halide Perovskites. *ACS Energy Lett.* **2017**, *2*, 1507−1514.
(25) Knight, A. J.; Wright, A. D.; Patel, J. B.; McMeekin, D. P.; Snaith, H. J.; Johnston, M. B.; Herz, L. M. Electronic Traps and Phase Segregation in Lead Mixed-Halide Perovskite. *ACS Energy Lett.* **2019**, *4*, 75−84.
(26) Cappel, U. B.; Svanström, S.; Lanzilotto, V.; Johansson, F. O. L.; Aitola, K.; Philippe, B.; Giangrisostomi, E.; Ovsyannikov, R.; Leitner, T.; Föhlisch, A.; Svensson, S.; Mårtensson, N.; Boschloo, G.; Lindblad, A.; Rensmo, H. Partially Reversible Photoinduced Chemical Changes in a Mixed-Ion Perovskite Material for Solar Cells. *ACS Appl. Mater. Interfaces* **2017**, *9*, 34970−34978.
(27) Balakrishna, R. G.; Kobosko, S. M.; Kamat, P. V. Mixed Halide Perovskite Solar Cells. Consequence of Iodide Treatment on Phase Segregation Recovery. *ACS Energy Lett.* **2018**, *3*, 2267−2272.
(28) Brennan, M. C.; Draguta, S.; Kamat, P. V.; Kuno, M. Light-Induced Anion Phase Segregation in Mixed Halide Perovskites. *ACS Energy Lett.* **2018**, *3*, 204−213.
(29) Correa-Baena, J.-P.; Luo, Y.; Brenner, T. M.; Snaider, J.; Sun, S.; Li, X.; Jensen, M. A.; Hartono, N. T. P.; Nienhaus, L.; Wieghold, S.; Poindexter, J. R.; Wang, S.; Meng, Y. S.; Wang, T.; Lai, B.; Holt, M. V.;


https://dx.doi.org/10.1021/acsaem.0c03191
ACS Appl. Energy Mater. 2021, 4, 2616−2628

Cai, Z.; Bawendi, M. G.; Huang, L.; Buonassisi, T.; Fenning, D. P. Homogenized Halides and Alkali Cation Segregation in Alloyed Organic-Inorganic Perovskites. *Science* **2019**, *363*, 627−631.
(30) Jiang, Q.; Zhao, Y.; Zhang, X.; Yang, X.; Chen, Y.; Chu, Z.; Ye, Q.; Li, X.; Yin, Z.; You, J. Surface Passivation of Perovskite Film for Efficient Solar Cells. *Nat. Photonics* **2019**, *13*, 460−466.
(31) Ferdani, D. W.; Pering, S. R.; Ghosh, D.; Kubiak, P.; Walker, A. B.; Lewis, S. E.; Johnson, A. L.; Baker, P. J.; Islam, M. S.; Cameron, P. J. Partial Cation Substitution Reduces Iodide Ion Transport in Lead Iodide Perovskite Solar Cells. *Energy Environ. Sci.* **2019**, *12*, 2264−2272.
(32) Zhang, M.; Yun, J. S.; Ma, Q.; Zheng, J.; Lau, C. F. J.; Deng, X.; Kim, J.; Kim, D.; Seidel, J.; Green, M. A.; Huang, S.; Ho-Baillie, A. W. Y. High-Efficiency Rubidium-Incorporated Perovskite Solar Cells by Gas Quenching. *ACS Energy Lett.* **2017**, *2*, 438−444.
(33) Sun, Y.; Peng, J.; Chen, Y.; Yao, Y.; Liang, Z. Triple-Cation Mixed-Halide Perovskites: Towards Efficient, Annealing-Free and Air-Stable Solar Cells Enabled by $Pb(SCN)_2$ Additive. *Sci. Rep.* **2017**, *7*, 46193.
(34) Leijtens, T.; Prasanna, R.; Bush, K. A.; Eperon, G. E.; Raiford, J. A.; Gold-Parker, A.; Wolf, E. J.; Swifter, S. A.; Boyd, C. C.; Wang, H.-P.; Toney, M. F.; Bent, S. F.; McGehee, M. D. Tin-Lead Halide Perovskites with Improved Thermal and Air Stability for Efficient All-Perovskite Tandem Solar Cells. *Sustainable Energy Fuels* **2018**, *2*, 2450−2459.
(35) Liao, W.; Zhao, D.; Yu, Y.; Shrestha, N.; Ghimire, K.; Grice, C. R.; Wang, C.; Xiao, Y.; Cimaroli, A. J.; Ellingson, R. J.; Podraza, N. J.; Zhu, K.; Xiong, R.-G.; Yan, Y. Fabrication of Efficient Low-Bandgap Perovskite Solar Cells by Combining Formamidinium Tin Iodide with Methylammonium Lead Iodide. *J. Am. Chem. Soc.* **2016**, *138*, 12360−12363.
(36) Eperon, G. E.; Leijtens, T.; Bush, K. A.; Prasanna, R.; Green, T.; Wang, J. T.-W.; McMeekin, D. P.; Volonakis, G.; Milot, R. L.; May, R.; Palmstrom, A.; Slotcavage, D. J.; Belisle, R. A.; Patel, J. B.; Parrott, E. S.; Sutton, R. J.; Ma, W.; Moghadam, F.; Conings, B.; Babayigit, A.; Boyen, H.-G.; Bent, S.; Giustino, F.; Herz, L. M.; Johnston, M. B.; McGehee, M. D.; Snaith, H. J. Perovskite-Perovskite Tandem Photovoltaics with Optimized Band Gaps. *Science* **2016**, *354*, 861−865.
(37) Nie, W.; Tsai, H.; Asadpour, R.; Blancon, J.-C.; Neukirch, A. J.; Gupta, G.; Crochet, J. J.; Chhowalla, M.; Tretiak, S.; Alam, M. A.; Wang, H.-L.; Mohite, A. D.; Belisle, R. A.; Patel, J. B.; Parrott, E. S.; Sutton, R. J.; Ma, W.; Moghadam, F.; Conings, B.; Babayigit, A.; Boyen, H. G.; Bent, S.; Giustino, F.; Herz, L. M.; Johnston, M. B.; McGehee, M. D.; Snaith, H. J. High-Efficiency Solution-Processed Perovskite Solar Cells with Millimeter-Scale Grains. *Science* **2015**, *347*, 522−525.
(38) Castro-Méndez, A.-F.; Hidalgo, J.; Correa-Baena, J. The Role of Grain Boundaries in Perovskite Solar Cells. *Adv. Energy Mater.* **2019**, *9*, 1901489.
(39) Wieghold, S.; Correa-Baena, J.-P.; Nienhaus, L.; Sun, S.; Shulenberger, K. E.; Liu, Z.; Tresback, J. S.; Shin, S. S.; Bawendi, M. G.; Buonassisi, T. Precursor Concentration Affects Grain Size, Crystal Orientation, and Local Performance in Mixed-Ion Lead Perovskite Solar Cells. *ACS Appl. Energy Mater.* **2018**, *1*, 6801−6808.
(40) Lee, D. S.; Yun, J. S.; Kim, J.; Soufiani, A. M.; Chen, S.; Cho, Y.; Deng, X.; Seidel, J.; Lim, S.; Huang, S.; Ho-Baillie, A. W. Y. Passivation of Grain Boundaries by Phenethylammonium in Formamidinium-Methylammonium Lead Halide Perovskite Solar Cells. *ACS Energy Lett.* **2018**, *3*, 647−654.
(41) Cho, Y.; Soufiani, A. M.; Yun, J. S.; Kim, J.; Lee, D. S.; Seidel, J.; Deng, X.; Green, M. A.; Huang, S.; Ho-Baillie, A. W. Y. Mixed 3D−2D Passivation Treatment for Mixed-Cation Lead Mixed-Halide Perovskite Solar Cells for Higher Efficiency and Better Stability. *Adv. Energy Mater.* **2018**, *8*, 1703392.
(42) Li, J.; Huang, B.; Nasr Esfahani, E.; Wei, L.; Yao, J.; Zhao, J.; Chen, W. Touching Is Believing: Interrogating Halide Perovskite Solar Cells at the Nanoscale via Scanning Probe Microscopy. *npj Quantum Mater.* **2017**, *2*, 56.
(43) Hills-Kimball, K.; Nagaoka, Y.; Cao, C.; Chaykovsky, E.; Chen, O. Synthesis of Formamidinium Lead Halide Perovskite Nanocrystals through Solid-Liquid-Solid Cation Exchange. *J. Mater. Chem. C* **2017**, *5*, 5680−5684.
(44) Mosconi, E.; Quarti, C.; Ivanovska, T.; Ruani, G.; De Angelis, F. Structural and Electronic Properties of Organo-Halide Lead Perovskites: A Combined IR-Spectroscopy and Ab Initio Molecular Dynamics Investigation. *Phys. Chem. Chem. Phys.* **2014**, *16*, 16137−16144.
(45) Szostak, R.; Silva, J. C.; Turren-Cruz, S.-H.; Soares, M. M.; Freitas, R. O.; Hagfeldt, A.; Tolentino, H. C. N.; Nogueira, A. F. Nanoscale Mapping of Chemical Composition in Organic-Inorganic Hybrid Perovskite Films. *Sci. Adv.* **2019**, *5*, No. eaaw6619.
(46) Coates, J. Interpretation of Infrared Spectra, A Practical Approach. *Encyclopedia of Analytical Chemistry*; Wiley, 2006.
(47) Chae, J.; Dong, Q.; Huang, J.; Centrone, A. Chloride Incorporation Process in $CH_3NH_3PbI_{3-x}Cl_x$ Perovskites via Nanoscale Bandgap Maps. *Nano Lett.* **2015**, *15*, 8114−8121.
(48) Hartono, N. T. P.; Sun, S.; Gélvez-Rueda, M. C.; Pierone, P. J.; Erodici, M. P.; Yoo, J.; Wei, F.; Bawendi, M.; Grozema, F. C.; Sher, M.-j.; Buonassisi, T.; Correa-Baena, J.-P. The Effect of Structural Dimensionality on Carrier Mobility in Lead-Halide Perovskites. *J. Mater. Chem. A* **2019**, *7*, 23949−23957.
(49) Wang, Z.; Lin, Q.; Chmiel, F. P.; Sakai, N.; Herz, L. M.; Snaith, H. J. Efficient Ambient-Air-Stable Solar Cells with 2D-3D Heterostructured Butylammonium-Caesium-Formamidinium Lead Halide Perovskites. *Nat. Energy* **2017**, *2*, 17135.
(50) Thouin, F.; Srimath Kandada, A. R.; Valverde-Chávez, D. A.; Cortecchia, D.; Bargigia, I.; Petrozza, A.; Yang, X.; Bittner, E. R.; Silva, C. Electron-Phonon Couplings Inherent in Polarons Drive Exciton Dynamics in Two-Dimensional Metal-Halide Perovskites. *Chem. Mater.* **2019**, *31*, 7085−7091.
(51) Manser, J. S.; Kamat, P. V. Band Filling with Free Charge Carriers in Organometal Halide Perovskites. *Nat. Photonics* **2014**, *8*, 737−743.
(52) Jacobsson, T. J.; Correa-Baena, J.-P.; Halvani Anaraki, E.; Philippe, B.; Stranks, S. D.; Bouduban, M. E. F.; Tress, W.; Schenk, K.; Teuscher, J.; Moser, J.-E.; Rensmo, H.; Hagfeldt, A. Unreacted $PbI_2$ as a Double-Edged Sword for Enhancing the Performance of Perovskite Solar Cells. *J. Am. Chem. Soc.* **2016**, *138*, 10331−10343.
(53) Price, M. B.; Butkus, J.; Jellicoe, T. C.; Sadhanala, A.; Briane, A.; Halpert, J. E.; Broch, K.; Hodgkiss, J. M.; Friend, R. H.; Deschler, F. Hot-Carrier Cooling and Photoinduced Refractive Index Changes in Organic-Inorganic Lead Halide Perovskites. *Nat. Commun.* **2015**, *6*, 8420.
(54) Droseros, N.; Dänekamp, B.; Tsokkou, D.; Boix, P. P.; Banerji, N. Charge Injection and Trapping at Perovskite Interfaces with Organic Hole Transporting Materials of Different Ionization Energies. *APL Mater.* **2019**, *7*, 041115.
(55) Shao, S.; Liu, J.; Portale, G.; Fang, H. H.; Blake, G. R.; ten Brink, G. H.; Koster, L. J. A.; Loi, M. A. Highly Reproducible Sn-Based Hybrid Perovskite Solar Cells with 9% Efficiency. *Adv. Energy Mater.* **2018**, *8*, 1702019.
(56) Jones, T. W.; Osherov, A.; Alsari, M.; Sponseller, M.; Duck, B. C.; Jung, Y.-K.; Settens, C.; Niroui, F.; Brenes, R.; Stan, C. V.; Li, Y.; Abdi-Jalebi, M.; Tamura, N.; Macdonald, J. E.; Burghammer, M.; Friend, R. H.; Bulović, V.; Walsh, A.; Wilson, G. J.; Lilliu, S.; Stranks, S. D. Lattice Strain Causes Non-Radiative Losses in Halide Perovskites. *Energy Environ. Sci.* **2019**, *12*, 596−606.
(57) Elmelund, T.; Seger, B.; Kuno, M.; Kamat, P. V. How Interplay between Photo and Thermal Activation Dictates Halide Ion Segregation in Mixed Halide Perovskites. *ACS Energy Lett.* **2020**, *5*, 56−63.
(58) Kamat, M. C.; Ruth, A.; Kamat, P. V.; Kuno, M. Photoinduced Anion Segregation in Mixed Halide Perovskites. *Trends Chem.* **2020**, *2*, 282−301.
(59) Prasanna, R.; Gold-Parker, A.; Leijtens, T.; Conings, B.; Babayigit, A.; Boyen, H.-G.; Toney, M. F.; McGehee, M. D. Band Gap Tuning via Lattice Contraction and Octahedral Tilting in Perovskite Materials for Photovoltaics. *J. Am. Chem. Soc.* **2017**, *139*, 11117−11124.


https://dx.doi.org/10.1021/acsaem.0c03191
*ACS Appl. Energy Mater.* 2021, 4, 2616−2628

(60) Saliba, M.; Etgar, L. Current Density Mismatch in Perovskite Solar Cells. *ACS Energy Lett.* **2020**, *5*, 2886−2888.
(61) Chen, B.; Yang, M.; Priya, S.; Zhu, K. Origin of J-V Hysteresis in Perovskite Solar Cells. *J. Phys. Chem. Lett.* **2016**, *7*, 905−917.
(62) Draguta, S.; Sharia, O.; Yoon, S. J.; Brennan, M. C.; Morozov, Y. V.; Manser, J. M.; Kamat, P. V.; Schneider, W. F.; Kuno, M. Rationalizing the Light-Induced Phase Separation of Mixed Halide Organic-Inorganic Perovskites. *Nat. Commun.* **2017**, *8*, 200.
(63) Beal, R. E.; Hagström, N. Z.; Barrier, J.; Gold-Parker, A.; Prasanna, R.; Bush, K. A.; Passarello, D.; Schelhas, L. T.; Brüning, K.; Tassone, C. J.; Steinrück, H.-G.; McGehee, M. D.; Toney, M. F.; Nogueira, A. F. Structural Origins of Light-Induced Phase Segregation in Organic-Inorganic Halide Perovskite Photovoltaic Materials. *Matter* **2020**, *2*, 207−219.
(64) Mahesh, S.; Ball, J. M.; Oliver, R. D. J.; McMeekin, D. P.; Nayak, P. K.; Johnston, M. B.; Snaith, H. J. Revealing the Origin of Voltage Loss in Mixed-Halide Perovskite Solar Cells. *Energy Environ. Sci.* **2020**, *13*, 258−267.
(65) Correa Baena, J. P.; Steier, L.; Tress, W.; Saliba, M.; Neutzner, S.; Matsui, T.; Giordano, F.; Jacobsson, T. J.; Srimath Kandada, A. R.; Zakeeruddin, S. M.; Petrozza, A.; Abate, A.; Nazeeruddin, M. K.; Grätzel, M.; Hagfeldt, A. Highly Efficient Planar Perovskite Solar Cells through Band Alignment Engineering. *Energy Environ. Sci.* **2015**, *8*, 2928−2934.
(66) Tao, S.; Schmidt, I.; Brocks, G.; Jiang, J.; Tranca, I.; Meerholz, K.; Olthof, S. Absolute Energy Level Positions in Tin- and Lead-Based Halide Perovskites. *Nat. Commun.* **2019**, *10*, 2560.
(67) Quarti, C.; De Angelis, F.; Beljonne, D. Influence of Surface Termination on the Energy Level Alignment at the $CH_3NH_3PbI_3$ Perovskite/$C_{60}$ Interface. *Chem. Mater.* **2017**, *29*, 958−968.
(68) Yao, D.; Zhang, C.; Zhang, S.; Yang, Y.; Du, A.; Waclawik, E.; Yu, X.; Wilson, G. J.; Wang, H. 2D−3D Mixed Organic−Inorganic Perovskite Layers for Solar Cells with Enhanced Efficiency and Stability Induced by n -Propylammonium Iodide Additives. *ACS Appl. Mater. Interfaces* **2019**, *11*, 29753−29764.
(69) Ye, M.; He, C.; Iocozzia, J.; Liu, X.; Cui, X.; Meng, X.; Rager, M.; Hong, X.; Liu, X.; Lin, Z. Recent Advances in Interfacial Engineering of Perovskite Solar Cells. *J. Phys. D: Appl. Phys.* **2017**, *50*, 373002.
(70) Liu, Z.; Ojima, H.; Hong, Z.; Kido, J.; Tian, W.; Wang, X.-F. Solution-Processed Organic Photovoltaics Based on Indoline Dye Molecules Developed in Dye-Sensitized Solar Cells. *Molecules* **2013**, *18*, 3107−3117.


https://dx.doi.org/10.1021/acsaem.0c03191
*ACS Appl. Energy Mater.* 2021, 4, 2616−2628